PHYSICAL CONDITIONS DERIVED FROM O II RECOMBINATION LINES IN PLANETARY NEBULAE AND THEIR IMPLICATIONS

A. Peimbert,[1] M. Peimbert,[1] G. Delgado-Inglada,[1] J. García-Rojas,[2] and M. Peña[1]

RESUMEN

A partir de observaciones de alta calidad del multiplete V1 de O II estudiamos la densidad y la temperatura de una muestra de nebulosas planetarias. Encontramos que, en general, las densidades que obtenemos a partir de las líneas de O II son similares a las densidades obtenidas a partir de líneas prohibidas. Esto implica que no hay evidencia de condensaciones de alta densidad y baja temperatura para la mayoría de los objetos de nuestra muestra. Las presiones electrónicas encontradas en las zonas calientes son semejantes o ligeramente mayores que las de las zonas frías, sugiriendo la presencia de ondas de choque. Las temperaturas promedio y los valores de t^2 obtenidos a partir de líneas de H, He y O son similares y consistentes con un medio químicamente homogéneo. Estos resultados sugieren que las abundancias obtenidas a partir de las líneas de recombinación son las representativas de estos objetos.

ABSTRACT

Based on high quality observations of multiplet V1 of O II and the NLTE atomic computations for O II we study the density and temperature of a sample of PNe. We find that, in general, the densities derived from recombination lines of O II are similar to the densities derived from forbidden lines. This implies that the signature for oxygen rich clumps of high density and low temperature is absent in most of the objects of our sample. Electron pressures derived from the hotter zones are similar or slightly larger than those derived from the colder zones, suggesting the presence of shock waves. The average temperatures and t^2 values derived from H, He and O lines are similar and consistent with chemical homogeneity. These results suggest that the abundances of these objects are the ones derived from recombination lines.

Key Words: ISM: abundances — planetary nebulae: general

1. INTRODUCTION

O/H abundance ratios derived from recombination lines of O and H are higher than those derived from the ratio of a collisionally excited line (CL) of oxygen to a recombination line (RL) of H. This effect is called the abundance discrepancy problem, and the ratio of both types of abundances is called the abundance discrepancy factor (ADF). This problem also applies to other heavy elements like C, N, and Ne and is present in H II regions as well as in planetary nebulae.

The two main explanations for the large ADF values found in planetary nebulae are: (a) the presence of large temperature variations, larger than those predicted by photoionized models such as CLOUDY (Ferland et al. 2013) in a chemically homogeneous medium (e.g., Peimbert & Peimbert 2006, and references therein), and (b) the presence of large temperature variations due to chemical inhomogeneities (e.g.,

Liu 2006, and references therein). Both explanations rely on the fact that RLs are inversely proportional to the temperature and in colder regions become brighter relatively to CLs, while CLs increase with temperature and become brighter relatively to RLs in hotter regions. In addition CLs in the visual range of the spectrum are almost non-existent in very cold regions ($T_e \lesssim 2000$ K).

In a chemically homogeneous medium $I(\text{O,RL})/I(\text{H,RL})$ is proportional to the O/H ratio and is almost independent of the electron temperature. Alternatively $I(\text{O,CL})/I(\text{H,RL})$ depends strongly on the electron temperature in such a way that, in the presence of temperature variations, the O/H abundances derived from temperature determinations based on CLs, assuming constant temperature, are underestimated giving rise to the presence of an ADF.

In a chemically inhomogeneous medium CLs are expected to originate mainly in regions that are relatively metal-poor, temperature-high and density-low, while the RLs are expected to originate mainly in re-

---

[1]Instituto de Astronomía, Universidad Nacional Autónoma de México, Mexico.

[2]Instituto de Astrofísica de Canarias (IAC), Spain.

gions that are relatively metal-rich, temperature-low, and density-high.

There are many heavy element line ratios that can be used to determine the physical characteristics of a photoionized region using CLs (i.e. capable of characterizing the hottest parts of photoionized regions). But until recently there were no heavy element RL ratios capable of determining physical conditions (i.e. capable of characterizing the coldest parts of photoionized regions). It is difficult, but possible, to determine physical conditions using light element RL ratios; this suggests moderate thermal inhomogeneities for H and He, but cannot discriminate between moderate or large thermal inhomogeneities for heavy elements, since, in the presence of chemical inhomogeneities, the physical determinations made for H or He would not be applicable to O, N, Ne, or C.

A decade ago Ruiz et al. (2003), Peimbert & Peimbert (2005) and Peimbert et al. (2005) observationally found that the O II V1 multiplet was not in local thermal equilibrium, a result that was theoretically confirmed later by Bastin & Storey (2006). The atomic physics taking into account the density dependence of the level populations of the ground states of the O II V1 multiplet has been computed by Storey (Bastin & Storey 2006; Liu 2012; Fang & Liu 2013), and is the one used in this paper.

The O II V1 multiplet consists of 8 lines emitted from atoms in the 4 energy levels of the O II $1s^2\ 2p^2$ (3P) 3p configuration that decay to the 3 energy levels of the O II $1s^2\ 2p^2$ (3P) 3s configuration. Since the multiplet is optically thin, if one can obtain at least one of the lines coming from each one of the 4 upper levels it is enough to fully characterize the emission from the 8 lines of the multiplet. The lines arising from each level are: from O II $2p^2$ (3P) 3p1 1/2 $\lambda\lambda$ 4651 and 4673; from O II $2p^2$ (3P) 3p1 3/2 $\lambda\lambda$ 4638, 4662, and 4696; from O II $2p^2$ (3P) 3p1 5/2 $\lambda\lambda$ 4642 and 4676; and from O II $2p^2$ (3P) 3p1 7/2 $\lambda\lambda$ 4649. In LTE the intensity of $\lambda(4649)$ is expected to be 39.7% of that of the multiplet (Wiese et al. 1996). When densities are lower than $n_e \approx 25000$ cm^{-3} this line becomes weaker dropping to 10% of the multiplet for very low densities. Since O II $\lambda4649$ was expected to be the brightest line of the multiplet, and since the lines of the multiplet are all very faint, many studies focused on measuring only the O II $\lambda4649$ line; unfortunately, for most photoionized regions, this results in underestimating the oxygen RL abundances by factors of up to 4 if the LTE predictions are adopted (Peimbert et al. 2005).

Recent calculations by Storey (presented by Peimbert & Peimbert 2013, hereafter PP13, and Fang & Liu 2013) allow the study of the temperature and density dependance of the O II V1 multiplet ratios. These calculations indicate that the individual line intensities are density and temperature dependent, while the sum is only temperature dependent. So far this is the only multiplet where the line by line density dependence has been characterized by both observations and atomic physics calculations.

PP13 studied the relevance of the O II V1 recombination lines for the determination of the physical conditions of H II regions. They considered nine galactic and extragalactic H II regions with high quality line intensity observations. They found that, for these objects, the densities derived from CLs (i.e. the densities in the hotter zones of the nebulae) are higher than the densities derived from RLs (i.e. the densities in the colder zones); this, together with an analysis of the temperature structure derived from H, He, and O, shows that high metallicity inclusions do not contribute much to the observed ADFs in HII regions; it also suggests that shock waves do contribute importantly to the ADF presence.

We decided to carry out a similar study to that of PP13 based on the best observed planetary nebulae trying to find out if these objects are chemically homogeneous or not and, in general, to study which physical processes are important as sources of thermal inhomogeneities in ionized nebulae.

2. THE SAMPLE

We selected from the literature 20 PNe with high quality spectra, both in terms of resolution and signal to noise ratio. The objective was to look for objects where enough lines of the O II V1 multiplet were measured with high signal to noise ratio, to properly characterize the whole multiplet, i.e., at least one line from each of the four upper levels that produce this multiplet.

Table 1 lists the studied PNe, the intensity ratios involving RLs of the O II V1 multiplet, and the references from which we took the emission line fluxes; F1 stands for the sum of the intensities of the [O III] $\lambda4959$ and [O III] $\lambda5007$ lines of multiplet F1.

The objects with the best O II intensity measurements available from the literature produce two selection effects on our sample: (a) Wesson, Liu and collaborators were interested in PNe with high ADF values (8 objects), and (b) García-Rojas and collaborators were interested in PNe with [WC] central stars or with weak emission line central stars (11 objects).

These two biases imply that the sample presented in this paper may not be representative of the total family of PNe, in the sense that the average ADF value for a more general sample could be smaller than for this sample. To advance further in this subject, it would be important to obtain additional observations of similar or higher quality than those used in this paper.

There are other line ratios of O II recombination lines that can be used to determine densities and temperatures, see Fang & Liu (2013). Unfortunately, one

TABLE 1

SAMPLE OF PNE AND LINE INTENSITY RATIOS

Object	$\frac{I(\mathrm{V1})^{\mathrm{a}}}{I(\mathrm{F1})}$	$\frac{I(4649)^{\mathrm{b}}}{I(4639+51+62)}$	Ref.[c]
Cn 1-5	97±12	115±29	(1)
He 2-86	122±4	122±6	(1)
Hu 1-1	28±11	76±37	(2)
Hu 2-1	116±9	136±16	(2)
M 1-25	158±15	82±17	(1)
M 1-30	454±20	92±9	(1)
M 1-61	80±4	120±19	(1)
M 3-15	149±22	87±28	(1)
NGC 2867	51±2	41±5	(3)
NGC 5189	39±4	61±13	(1)
NGC 5307	38±4	73±15	(4)
NGC 6153	346±10	106±5	(5)
NGC 6803	89±5	116±12	(2)
NGC 6879	56±12	30±14	(2)
NGC 6891	68±5	68±14	(2)
NGC 7009	133±10	92±11	(6)
NGC 7026	110±5	106±11	(2)
PB 8	365±16	71±8	(3)
PC 14	82±6	88±12	(1)
Pe 1-1	57±4	127±30	(1)

[a]In units of 10^{-5}.

[b]In units of 10^{-2}.

[c]References: (1) García-Rojas et al. (2012), (2) Wesson et al. (2005), (3) García-Rojas et al. (2009), (4) Ruiz et al. (2003), (5) Liu et al. (2000), (6) Fang & Liu (2011).

or both of the lines involved are at least one order of magnitude fainter than the V1 lines, and therefore the measured line intensities present larger errors. In addition, at that level of intensity and with the spectral resolutions available, it is not possible to separate the contribution due to other, weaker, lines that could be contributing to the measured line intensities.

3. PHYSICAL CONDITIONS

3.1. *Temperature determinations based on O II recombination lines*

Based on the atomic data for case B by Storey (1994), Storey & Zeippen (2000), and Storey et al. (2014) we find that

$$\frac{I(\mathrm{V1})}{I(\mathrm{F1})} =$$

$$1.772 \times 10^{-5} \left(\frac{T_{\mathrm{e}}}{10000\,\mathrm{K}} \right)^{-0.40} \exp(29170\,\mathrm{K}/T_{\mathrm{e}}). \quad (1)$$

TABLE 2

PHYSICAL CONDITIONS OF THE COLD ZONES

Object	$T_{\mathrm{e}}(\mathrm{V1/F1})$	$n_{\mathrm{e}}(\mathrm{O\,II})$
Cn 1-5	7500±195	$8880^{+\infty}_{-5130}$
He 2-86	7120±55	13300^{+6730}_{-3590}
Hu 1-1	9790±740	2480^{+6240}_{-1350}
Hu 2-1	7270±125	$49790^{+\infty}_{-37040}$
M 1-25	6740±125	2500^{+2110}_{-890}
M 1-30	5500±40	3230^{+1320}_{-820}
M 1-61	7860±100	$11760^{+154500}_{-6120}$
M 3-15	6810±200	3030^{+5640}_{-1490}
NGC 2867	8850±120	710^{+160}_{-130}
NGC 5189	9510±260	1530^{+770}_{-470}
NGC 5307	9600±250	2210^{+1280}_{-690}
NGC 6153	5800±30	5540^{+1160}_{-940}
NGC 6803	7540±70	9360^{+10240}_{-3420}
NGC 6879	7930±290	400^{+380}_{-240}
NGC 6891	8460±165	1800^{+940}_{-550}
NGC 7009	6990±115	3590^{+1660}_{-1020}
NGC 7026	7160±70	5890^{+4160}_{-1840}
PB 8	5710±45	1630^{+450}_{-340}
PC 14	7810±125	3290^{+1680}_{-970}
Pe 1-1	8550±135	$17400^{+\infty}_{-11920}$

We will call $T_{\mathrm{e}}(\mathrm{V1/F1})$ the temperature derived from equation (1). These temperatures are presented in Table 2.

Equation (1) is density independent because the sum of the intensities of the eight lines of multiplet V1 is density independent. Moreover, equation (1) is different from equation (6) in PP13 for two reasons: (a) we include the [O III] $\lambda 5007$ line in the calculations, and (b) the equation in PP13 had a misprint, $T_{\mathrm{e}}^{-0.415}$ should have been $(T_{\mathrm{e}}/10000\,\mathrm{K})^{-0.415}$.

The nebular lines have a much weaker temperature dependence than the auroral lines; the V1 multiplet temperature dependence is approximately equally strong to that of the nebular lines, but biased towards colder temperatures. Therefore, in the presence of temperature inhomogeneities, $T_{\mathrm{e}}(\mathrm{V1/F1})$ will represent better the cold zones of the nebulae than the normal auroral versus nebular temperatures, so we will use $T_{\mathrm{e}}(\mathrm{V1/F1})$ to represent them.

3.2. *Density determinations based on O II recombination lines*

It is possible to determine densities using only lines from the O II V1 multiplet (Ruiz et al. 2003). From Figure 3 of PP13, which is based on the unpublished computations by Storey (Bastin & Storey 2006; Liu 2012; Fang & Liu 2013), and the $I(4649)/I(4639+51+62)$ ratio presented in Table 1, we have computed the $n_e(\mathrm{O\,II})$ values presented in Ta-

TABLE 3

PHYSICAL CONDITIONS OF THE HOT ZONES AND PRESSURE
RATIOS BETWEEN THE HOT AND COLD ZONES

Object	T_e([O III])	n_e([Cl III])	$\log P(\text{hz})/P(\text{cz})$
Cn 1-5	8850±165	3400^{+800}_{-700}	$-0.36^{+0.38}_{-\infty}$
He 2-86	8500±150	17350^{+4300}_{-3100}	$0.18^{+0.15}_{-0.23}$
Hu 1-1	11870±270	1500±300	$-0.14^{+0.35}_{-0.56}$
Hu 2-1	10890±260	10600^{+9300}_{-4000}	$-0.50^{+0.61}_{-\infty}$
M 1-25	7840±145	11650^{+2200}_{-2100}	$0.75^{+0.21}_{-0.28}$
M 1-30	6650±150	6200^{+1300}_{-1000}	$0.37^{+0.15}_{-0.17}$
M 1-61	9260±200	16000^{+4300}_{-3200}	$0.18^{+0.33}_{-1.16}$
M 3-15	8400±225	7700^{+1800}_{-1400}	$0.49^{+0.30}_{-0.47}$
NGC 2867	11900±285	3800^{+900}_{-800}	$0.87±0.13$
NGC 5189	11670±280	1150^{+500}_{-400}	$-0.04^{+0.22}_{-0.27}$
NGC 5307	11770±90	1600^{+950}_{-850}	$0.13^{+0.18}_{-0.21}$
NGC 6153	9120±155	3550^{+700}_{-600}	$-0.003^{+0.11}_{-0.13}$
NGC 6803	9650±180	8700^{+1600}_{-1200}	$0.08^{+0.21}_{-0.33}$
NGC 6879	12010±270	4450^{+1100}_{-700}	$1.23^{+0.40}_{-0.31}$
NGC 6891	9180±160	1850±400	$0.05^{+0.18}_{-0.21}$
NGC 7009	9900±180	3400±200	$0.12^{+0.15}_{-0.17}$
NGC 7026	9390±165	8800^{+1500}_{-1300}	$0.29^{+0.18}_{-0.24}$
PB 8	6940±110	1750^{+1400}_{-900}	$0.16^{+0.21}_{-0.56}$
PC 14	9370±170	2900^{+800}_{-550}	$0.04^{+0.17}_{-0.21}$
Pe 1-1	10080±235	24000^{+7550}_{-5000}	$0.21^{+0.51}_{-\infty}$

ble 2. For those objects where this ratio is equal or higher than 1.15, and the error is greater than 10% (Cn 1-5, Hu 2-1, M 1-61, and Pe 1-1), the derived densities are very uncertain, with no real restriction on the upper limit.

For all the other objects, this determination requires a temperature to uniquely derive the density. Since RLs are brighter in the cold zones of photoionized regions, a colder temperature than the one derived from nebular versus auroral lines is required. For the chemically homogeneous model the correct temperature to use can be approximated by $T_e(V1/F1)$. In the presence of high-metallicity dense clumps a lower temperature should be used; with lower temperatures the derived densities will also be lower (see Figure 3 of PP13) by approximately $n_e \propto T_e^{2/3}$. We will discuss the implications of this result in § 4.

3.3. Temperature and densities based on collisionally excited lines

We have computed T_e([O III]) and n_e([Cl III]) as representative values of the temperature and density in the hot regions of the O^{++} zone. They were calculated from the [O III] $(\lambda4959+\lambda5007)/\lambda4363$ and [Cl III] $\lambda\lambda5517, 5537$ diagnostic ratios, respectively.

For the four PNe where [Cl III] lines were not available (Hu 1-1, Hu 2-1, NGC 6879, and NGC 6891), we adopted the average value of the densities obtained with three other diagnostic ratios: [O II] $\lambda3727/\lambda3729$, [S II] $\lambda6716/\lambda6731$, and [Ar IV] $\lambda4711/\lambda4740$. This assumption is reasonable, since for the other 16 PNe where all the diagnostic ratios are available, the agreement between the average density and the one obtained from chlorine lines is better than $\approx 30\%$.

All the calculations have been performed with the software PyNeb (Luridiana et al. 2012) and the uncertainties associated with the physical conditions have been computed through Montecarlo simulations. We adopted the transitions probabilities and the collision strengths from Mendoza & Zeippen (1982b) and Ramsbottom & Bell (1997) for Ar^{+3}, Mendoza & Zeippen (1982a) and Butler & Zeippen (1989) for Cl^{++}, Storey & Zeippen (2000) and Storey et al. (2014) for O^{++}, Wiese et al. (1996) and Kisielius et al. (2009) for O^+, and Zeippen (1982) and Tayal & Zatsarinny (2010) for S^+.

Table 3 shows the final temperatures and densities derived for each nebula. The differences between our values and those provided in the papers listed in Table 1 are about 3% for T_e and about 15% for n_e with
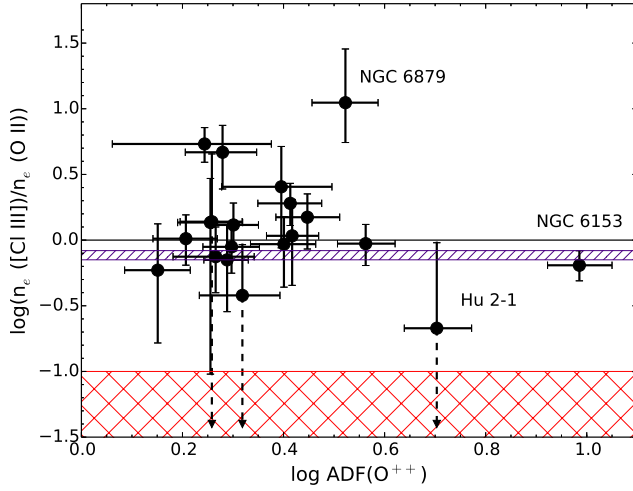
Fig. 1. Ratio of n_{e}([Cl III]) to n_{e}(O II) values as a function of ADF(O^{++}). The solid line shows where the values of n_{e}(O II) and n_{e}([Cl III]) are equal. The small dashed area represents a chemically homogeneous region of constant pressure. The crossed area at the bottom represents models with constant pressure in a chemically inhomogeneous medium where the metal poor regions are at least 10 times hotter than the metal rich regions.

a few exceptions showing higher differences. The differences are caused by the different sets of atomic data used in the calculations.

4. DENSITIES AND ADFs

Figure 1 shows the ratio of n_{e}(O II) to n_{e}([Cl III]) values as a function of the ADF(O^{++}), given by

$$\mathrm{ADF(O^{++})} = \frac{\mathrm{(O^{++}/H^+)_{RLs}}}{\mathrm{(O^{++}/H^+)_{CLs}}}. \qquad (2)$$

The values of O^{++}/H$^+$ from RLs were directly taken from the V1 multiplet abundances presented in the papers listed in Table 1. For those PNe where no uncertainties are provided by the authors we assume a one sigma error of ± 0.05 dex. The O^{++} abundances from CLs were computed with the [O III] $\lambda\lambda 4959$, 5007/Hβ intensity ratios and the physical conditions of Table 3. They are listed in Table 4 together with the ADF(O^{++}) values.

The ADF is present in all the objects of our sample. The ADF range goes from 1.42 (Hu 1-1) to 9.67 (NGC 6153), the average value being 2.74. If we eliminate the two objects with the highest ADF value, the range of the other 18 goes from 1.42 to 3.65 with an average value of 2.23. The average value would be probably smaller for a typical sample of PNe, because part of our sample is biased towards objects with high ADF values.

Two sets of models have been proposed to explain the ADF values: chemically inhomogeneous models and chemically homogeneous ones.

Chemically inhomogeneous models consist of pockets of high density and low temperature embedded in a medium of lower density and higher temperature. In these models most of the mass is located in the medium of lower density and higher temperature and consequently the proper abundances for heavy elements are those obtained from the intensity ratios of forbidden lines to hydrogen recombination lines.

A chemically homogeneous model requires the consideration of physical processes additional, to those given by direct ionization from the central star, to explain the observed ADF values. Four of these processes are: shocks, magnetic reconnection, shadowed ionization, and a receding ionization front.

In the presence of large temperature variations the ratio of a collisionally excited line to a recombination line depends strongly on the temperature. In the presence of temperature inhomogeneities when the temperature is derived from the ratio of two collisionally excited lines the abundances of the heavy elements derived from the ratio of a collisionally excited line to a hydrogen line are lower limits to the real abundance ratio (Peimbert 1967; Peimbert & Costero 1969).

On the other hand the recombination lines of the heavy elements and of hydrogen depend weakly on the electron temperature; they are inversely proportional to the temperature and to a very good approximation the intensity ratios of two recombination lines are almost independent of the average temperature as well as of the presence of temperature inhomogeneities. Therefore, in models with temperature inhomogeneities the proper abundances are those provided by recombination lines of the heavy elements to those of hydrogen.

From Tables 2 and 3 and Figure 1 it follows that six objects have n_{e}([Cl III]) higher than the n_{e}(O II) values and 11 objects have n_{e}([Cl III]) values that are consistent with the n_{e}(O II) values; the three other objects, Cn 1-5, Hu 2-1, and NGC 6153, are not compatible with density equilibrium but are consistent with pressure equilibrium. However, it cannot be ruled out at one sigma level that four objects (Cn 1-5, Hu 2-1, M 1-61, Pe 1-1) may have significantly low n_{e}([Cl III])/n_{e}(O II) ratios.

The minimum temperature that we are adopting for the n_{e}(O II) determinations is 5500 K. In the chemical inhomogeneous model the temperature of the cold zones is expected to be much lower than this value. The chemically inhomogeneous models are expected to be able to reproduce the observed V1/F1 ratio by having a much lower temperature in the cold zone. If the temperatures were lower than those adopted in this paper, the measured n_{e}(O II) value would decrease even

TABLE 4

O^{++} ABUNDANCES AND ADF

Object	$\{O^{++}\}^a_{RLs}$	$\{O^{++}\}_{CLs}$	$ADF(O^{++})$
Cn 1-5	8.99±0.06	8.67±0.04	$2.08^{+0.39}_{-0.37}$
He 2-86	9.02±0.02	8.72±0.04	$2.00^{+0.24}_{-0.20}$
Hu 1-1	8.57±0.05	8.42±0.04	$1.42^{+0.23}_{-0.20}$
Hu 2-1	8.73±0.05	8.03±0.04	$5.05^{+0.87}_{-0.69}$
M 1-25	8.89±0.05	8.61±0.04	$1.90^{+0.32}_{-0.30}$
M 1-30	8.92±0.03	8.51±0.05	$2.59^{+0.40}_{-0.36}$
M 1-61	8.88±0.04	8.62±0.04	$1.80^{+0.28}_{-0.25}$
M 3-15	9.17±0.09	8.77±0.05	$2.49^{+0.64}_{-0.59}$
NGC 2867	8.65±0.13	8.41±0.04	$1.75^{+0.62}_{-0.60}$
NGC 5189	8.66±0.06	8.40±0.04	$1.84^{+0.35}_{-0.33}$
NGC 5307	8.77±0.04	8.48±0.01	1.94±0.20
NGC 6153	9.61±0.05	8.62±0.04	$9.67^{+1.55}_{-1.31}$
NGC 6803	9.07±0.05	8.67±0.04	$2.52^{+0.39}_{-0.36}$
NGC 6879	8.82±0.05	8.30±0.04	$3.33^{+0.53}_{-0.47}$
NGC 6891	8.82±0.05	8.61±0.04	$1.61^{+0.25}_{-0.22}$
NGC 7009	9.18±0.05	8.62±0.02	$3.65^{+0.52}_{-0.44}$
NGC 7026	9.08±0.05	8.64±0.04	$2.80^{+0.44}_{-0.37}$
PB 8	9.15±0.03	8.73±0.04	$2.61^{+0.34}_{-0.29}$
PC 14	9.01±0.04	8.72±0.04	$1.98^{+0.27}_{-0.24}$
Pe 1-1	8.79±0.04	8.53±0.04	$1.81^{+0.27}_{-0.24}$

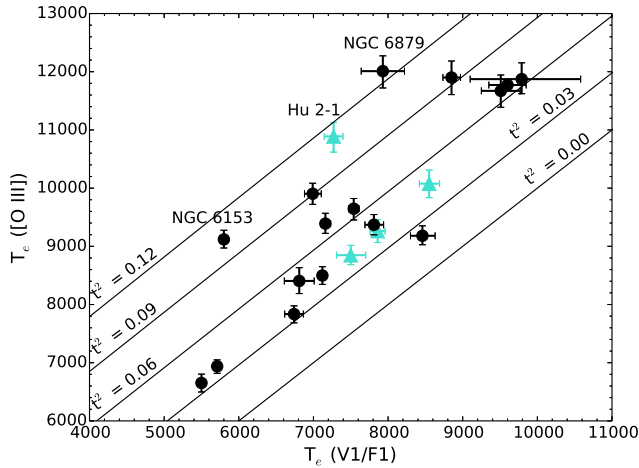[a]From the papers listed in Table 1.

Fig. 2. Comparison between $T_e([O\,III])$ and $T_e(V1/F1)$. The solid lines are sequences of equal t^2 values obtained from equations (6) and (7). The four triangles are the objects where we cannot discard the presence of chemical inhomogeneities (see Figure 1).

further. This is not compatible with the inhomogeneous models that usually require the densities of the cold zones to be at least one order of magnitude higher than those of the hot zones.

The other interesting point that follows from Figure 1 is that there is no correlation between $n_e([Cl\,III])/n_e(O\,II)$ and the $ADF(O^{++})$ value. For chemically inhomogeneous PNe it is expected that the higher the $ADF(O^{++})$ value the lower the $n_e([Cl\,III])/n_e(O\,II)$ ratio.

5. TEMPERATURE STRUCTURE

The $T_e([O\,III])/T_e(V1/F1)$ ratio varies in the 1.09 to 1.58 range with an average value of 1.28; the most extreme object is NGC 6153.

We decided to follow the formalism introduced by Peimbert (1967) to determine the basic parameters of the temperature structure, $T_0(O^{++})$ and $t^2(O^{++})$, where

$$T_0(O^{++}) = \frac{\int T_e n_e n(O^{++})dV}{\int n_e n(O^{++})dV}, \qquad (3)$$

and

$$t^2(O^{++}) = \frac{\int (T_e - T_0(O^{++}))^2 n_e n(O^{++})dV}{T_0(O^{++})^2 \int n_e n(O^{++})dV}. \qquad (4)$$

To study $T_0(O^{++})$ and $t^2(O^{++})$ we need an analytical expression for $T_e([O\,III])$. Based on the atomic data by Storey & Zeippen (2000); Storey et al. (2014) we find that

$$\frac{I(4363)}{I(F1)} = 0.1308 \exp(-32965\,K/T_e). \qquad (5)$$

From equations (1), (3), (4), and (5), and the temperature dependence of the emissivities ε_{V1}, ε_{4959}, and ε_{4363} (see PP13), we can write $T_e(V1/F1)$ and $T_e([O\,III])$ as a function of T_0 and t^2 as follows:

$$T_e([O\,III]) = T_0(O^{++})$$
$$\times \left[1 + \left(\frac{91305\,K}{T_0(O^{++})} - 2.74\right)\frac{t^2(O^{++})}{2}\right], \quad (6)$$

and

$$T_e(V1/F1) = T_0(O^{++}) \times \left[1 + \left(\frac{29170\,K}{T_0(O^{++})} - 3.14\right.\right.$$
$$\left.\left. + \frac{0.40}{\frac{29170\,K}{T_0(O^{++})} + 0.40}\right)\frac{t^2(O^{++})}{2}\right]. \qquad (7)$$

Using equations (6) and (7), along with the temperatures presented in Tables 2 and 3, we have derived the $T_0(O^{++})$ and $t^2(O^{++})$ values presented in Table 5.

Figure 2 shows the comparison between the temperatures of the hot zones, $T_e([O\,III])$, and the temperatures of the cold zones, $T_e(V1/F1)$. We overplot in the figure five sequences of equal t^2.

TABLE 5

OTHER TEMPERATURES AND t^2 VALUES

Object	$T_0(\mathrm{O}^{++})$	$T(\mathrm{Bac/Pac})$[a]	$t^2(\mathrm{O}^{++})$	$t^2(\mathrm{He\ I/CL})$[a]
Cn 1-5	7305±235	...	0.043±0.008	0.042±0.014
He 2-86	6905±70	7560^{+3050}_{-2060}	0.044±0.005	0.036±0.014
Hu 1-1	9700±780	8350	0.067±0.024	...
Hu 2-1	6735±180	8960	0.113±0.009	...
M 1-25	6545±155	7750^{+3100}_{-2050}	0.035±0.006	0.035±0.019
M 1-30	5240±60	5800^{+2150}_{-1300}	0.037±0.005	$0.013^{+0.018}_{-0.013}$
M 1-61	7675±120	9800^{+4150}_{-2700}	0.044±0.006	0.034±0.007
M 3-15	6560±255	9800^{+4150}_{-2800}	0.049±0.010	0.078±0.030
NGC 2867	8625±150	8950^{+2900}_{-1900}	0.096±0.007	0.046±0.029
NGC 5189	9390±295	9200^{+3600}_{-2300}	0.069±0.011	0.054±0.008
NGC 5307	9490±280	10700±2000	0.069±0.008	0.031±0.014
NGC 6153	5050±60	6080	0.105±0.005	...
NGC 6803	7250±90	7320	0.067±0.006	...
NGC 6879	7440±400	8500	0.128±0.012	...
NGC 6891	8350±185	5930	0.024±0.008	...
NGC 7009	6515±155	6490	0.092±0.007	...
NGC 7026	6820±95	7440	0.070±0.005	...
PB 8	5455±60	5100^{+1300}_{-900}	0.039±0.004	$0.008^{+0.020}_{-0.028}$
PC 14	7600±150	8500^{+3250}_{-2050}	0.050±0.007	0.040±0.004
Pe 1-1	8385±155	10300^{+4500}_{-2950}	0.051±0.009	0.044±0.007

[a]From the papers listed in Table 1.

This figure is based on the assumption that the chemical composition of each PNe of our sample is homogeneous. From this figure we find $t^2(\mathrm{O}^{++})$ values in the 0.024 to 0.128 range, a range similar to the one obtained from galactic and extragalactic H II regions by Peimbert et al. (2012), which amounts to $0.019 - 0.120$. The average $t^2(\mathrm{O}^{++})$ value of our sample is 0.0645, a value somewhat higher than that obtained from galactic and extragalactic H II regions by Peimbert et al. (2012) which amounts to 0.044.

The values of $t^2(\mathrm{O}^{++})$ calculated by us and the available $t^2(\mathrm{He\ I/CL})$ values from the literature are listed in Table 5.

For the 12 PNe of our sample with $t^2(\mathrm{He\ I/CL})$ values in the literature (those observed by García-Rojas et al. 2009, 2012 and Ruiz et al. 2003), the average $t^2(\mathrm{He\ I/CL})$ amounts to 0.042, in very good agreement with the average $t^2(\mathrm{O}^{++})$ which amounts to 0.045. This result supports the idea that O and He are well mixed in these objects.

6. THE ROLE OF PRESSURE

Physically, it is more meaningful to study the pressure ratio than the density ratio between the hot and cold zones in nebulae; therefore, we will proceed to determine the pressure ratio.

As in PP13, the electron pressures were derived through the ideal gas equation, $P_e = n_e k T_e$. The pressures of the cold zones, $P_e(\mathrm{cz})$, were obtained with $T_e(\mathrm{V1/F1})$ and $n_e(\mathrm{O\ II})$, whereas the pressures of the hot zones, $P_e(\mathrm{hz})$, were obtained with $T_e([\mathrm{O\ III}])$ and $n_e([\mathrm{Cl\ III}])$. The last column in Table 3 lists the ratio between both pressures for each nebula.

In the model with chemical inhomogeneities the predicted high density pockets of low temperature are expected to reach pressure equilibrium with the low density medium of high temperature. We find that in most of the objects $P_e(\mathrm{hz})$ is higher than $P_e(\mathrm{cz})$. This excess has two implications: (a) that probably it is due to the presence of shock waves, where we expect an increase of the temperature and the density, and (b) that the low densities found in the cold zones would require a very large fraction of the O^{++} in the cold zones to reproduce the observed recombination line intensities, contrary to the predictions of the chemical inhomogeneous models.

Figures 3–5 show the ratio of $P_e(\mathrm{hz})$ to $P_e(\mathrm{cz})$ values as a function of $n_e([\mathrm{Cl\ III}])$, ADF(O^{++}), and
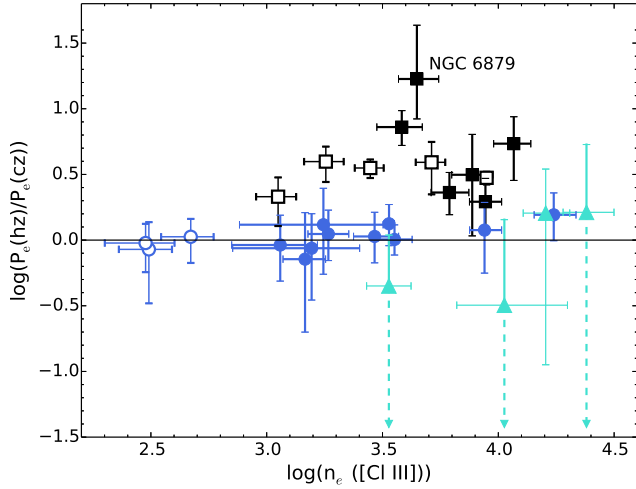
Fig. 3. Ratio between the pressure in the hot zones, $P_e(hz)$, and the pressure in the cold zones, $P_e(cz)$, as a function of $n_e([Cl\,III])$. The filled symbols represent PNe and the open ones H II regions. The squares represent the objects with pressure ratios strictly above zero. The circles are those objects with pressure ratios compatible with zero within errors. The four triangles are the objects where we cannot discard the presence of chemical inhomogeneities. The solid line shows where the pressures of the cold and hot zones are equal.

O^{++}/H^+ derived from RLs. For comparison we include the eight Galactic H II regions studied in PP13 (Esteban et al. 2004; García-Rojas et al. 2004, 2005, 2006, 2007).

From Figure 3 we see that nebulae with $n_e([Cl\,III])$ $\gtrsim 3200$ cm^{-3} show the largest departures from pressure equilibrium, while the objects with a relatively low density seem to be closer to pressure equilibrium than those with higher densities. A similar result was found for H II regions by PP13. As in H II regions, this result can be related to age of the nebulae.

The three PNe with the highest t^2 values are NGC 6879, Hu 2-1, and NGC 6153. The first one is the PN with the highest pressure ratio; for Hu 2-1 we cannot rule out the presence of high density and low temperature regions; and NGC 6153 shows pressure equilibrium. This indicates that there is no obvious correlation between temperature fluctuations and pressure equilibrium. This is also shown in Figure 5, where the pressure ratios and the ADF show no clear relation. In particular, the PN with the highest ADF, NGC 6153, presents similar pressures in the the hot and the cold zones.

The PNe and H II regions studied cover a wide range in $12+\log(O^{++}/H^+)$, from ≈ 8.08 (S311) to 9.61 (NGC 6153). There is no corelation between the pressure ratios and the O^{++} abundances.
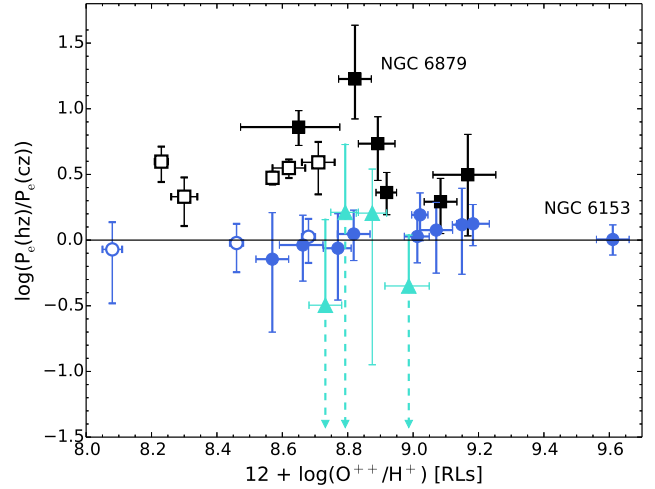

Fig. 4. Ratio between the pressure in the hot zones, $P_e(hz)$, and the pressure in the cold zones, $P_e(cz)$, as a function of O^{++}/H^+ derived from RLs. The symbols and the solid line are the same as in Figure 3.

The C/O and N/O abundance ratios reflect the effect of nucleosynthesis mechanisms in the progenitor stars of PNe, the asymptotic giant branch stars (AGB). Theoretical models by Karakas (2010) predict an increase of the nitrogen abundance in the most massive AGB stars, above $\approx 4\ M_\odot$ for a metallicity of Z = 0.02, as a consequence of the second dredge up. These models predict that the carbon abundance is not altered in the less massive progenitors with $M < 2.5\ M_\odot$; it increases in stars with $M \gtrsim 2.5\ M_\odot$ due to the third dredge up, and it may decrease in stars with $M \gtrsim 4\ M_\odot$ due to the hot bottom burning process. In Figures 6 and 7 we studied possible correlations between pressure ratios and these abundance ratios.

The C/O abundance ratios were computed from RLs. The ionic abundances of C^{++}, shown in Table 6, were directly taken from the papers listed in Table 1. For those PNe where no uncertainties are provided by the authors we assumed a one sigma error of ± 0.04 dex for the determination of C^{++}/H^+. To calculate the total C/O abundance ratios, we used the ICFs and the associated uncertainties from Delgado-Inglada et al. (2014), shown in Column (4) of Table 6.

Using CLs and the physical conditions given in Table 3, we computed the O^+, O^{++}, and N^+ abundances. We used the [O II] $\lambda 3727$, $\lambda 3729$ lines to compute O^+/H^+, the [O III] $\lambda 4959$, $\lambda 5007$ lines for O^{++}/H^+, and the [N II] $\lambda 6548$, $\lambda 6584$ lines for N^+/H^+. The final ionic abundances are the mean values from those derived with each line ratio. The values of N/O have been derived with the ICFs by Delgado-Inglada et al. (2014). Columns 2, 4, and 6 in Table 7 list the ionic and total abundances derived from CLs and $t^2 = 0$, whereas Columns 3, 5, and 7 show the values for $t^2 \neq 0$.

TABLE 6

IONIC ABUNDANCES[a], ICF(C^{++}/O^{++}), AND log(C/O) VALUES FROM RLS

Object	{C^{++}}	ICF	log(C/O)
Cn 1-5	9.08±0.02	0.95±$^{+0.05}_{-0.09}$	0.07$^{+0.09}_{-0.11}$
He 2-86	8.83±0.04	1.07±$^{+0.07}_{-0.09}$	−0.16$^{+0.08}_{-0.10}$
Hu 1-1	9.01±0.04	0.89±$^{+0.04}_{-0.09}$	0.39$^{+0.09}_{-0.12}$
Hu 2-1	8.66±0.04	0.81±$^{+0.03}_{-0.09}$	−0.16$^{+0.08}_{-0.12}$
M 1-25	8.75±0.02	0.77±$^{+0.02}_{-0.09}$	−0.26$^{+0.07}_{-0.11}$
M 1-30	8.93±0.01	0.64±$^{+0.03}_{-0.09}$	−0.18$^{+0.05}_{-0.10}$
M 1-61	8.64±0.03	1.06±$^{+0.07}_{-0.09}$	−0.20$^{+0.09}_{-0.11}$
M 3-15	8.84±0.04	1.14±$^{+0.08}_{-0.09}$	−0.27$^{+0.14}_{-0.13}$
NGC 2867	9.01±0.08	1.08±$^{+0.07}_{-0.09}$	0.39$^{+0.21}_{-0.18}$
NGC 5189	8.48±0.04	0.95±$^{+0.05}_{-0.09}$	−0.21$^{+0.09}_{-0.12}$
NGC 5307	7.95±0.10	1.20±$^{+0.26}_{-0.22}$	−0.74$^{+0.28}_{-0.26}$
NGC 6153	9.35±0.04	1.13±$^{+0.08}_{-0.09}$	−0.21$^{+0.11}_{-0.12}$
NGC 6803	8.79±0.04	1.11±$^{+0.08}_{-0.09}$	−0.24$^{+0.11}_{-0.12}$
NGC 6879	8.25±0.04	1.20±$^{+0.26}_{-0.22}$	−0.50$^{+0.27}_{-0.23}$
NGC 6891	8.74±0.04	1.17±$^{+0.09}_{-0.09}$	−0.01$^{+0.12}_{-0.12}$
NGC 7009	8.74±0.04	1.18±$^{+0.26}_{-0.22}$	−0.37$^{+0.27}_{-0.23}$
NGC 7026	8.98±0.04	1.04±$^{+0.06}_{-0.09}$	−0.09$^{+0.10}_{-0.12}$
PB 8	8.84±0.04	1.00±$^{+0.06}_{-0.09}$	−0.31$^{+0.10}_{-0.12}$
PC 14	8.91±0.03	1.12±$^{+0.08}_{-0.09}$	−0.05$^{+0.09}_{-0.10}$
Pe 1-1	9.02±0.02	0.92±$^{+0.04}_{-0.09}$	0.19$^{+0.07}_{-0.10}$

[a]{X^{+i}} = 12 + log(X^{+i}/H$^+$).

Figures 6 and 7 show that there is no obvious trend between the pressure ratios and the C/O or N/O abundance ratios. According to Peimbert (1990) about half of our sample are type I PNe, with log(N/O) > 0.5, which would arise from massive progenitor stars, whereas the other half are type II PNe, with log(N/O) < 0.5. As for the C/O values, most of the PNe show C/O > C/O$_\odot$ (where C/O$_\odot$ = 0.5; Allende Prieto et al. 2002) probably reflecting the occurrence of the third dredge up, but not of the hot bottom burning. Only three PNe have C/O < C/O$_\odot$: NGC 5307, NGC 6879, and NGC 7009. Since these three PNe also show low values of N/O, they probably arise from low mass progenitor stars ($M < 2\ M_\odot$).

7. HIGH DENSITY OBJECTS

There are four objects where we cannot rule out the presence of high density low temperature regions. They are Cn 1-5, Hu 2-1, M 1-61 and Pe 1-1. Three of these objects, Hu 2-1, M 1-61 and Pe 1-1, have a relatively high density, where our method to derive n_e(O II) is not very sensitive and presents large errors because it saturates at high densities (see Figure 3 of PP13). Cn 1-5

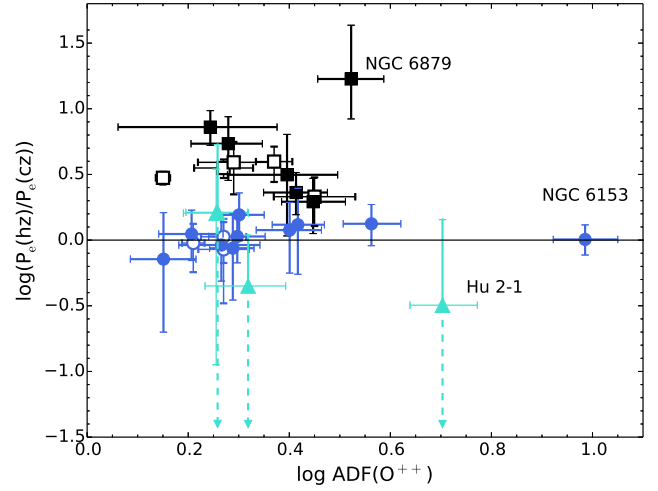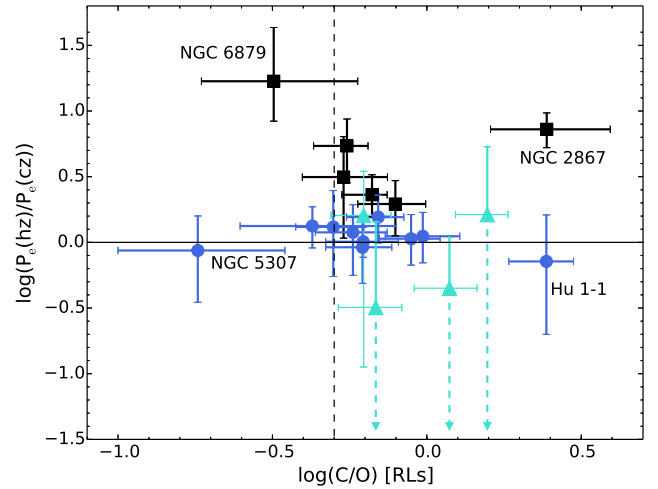Fig. 5. Ratio between the pressure in the hot zones, P_e(hz), and the pressure in the cold zones, P_e(cz), as a function of ADF(O^{++}). The symbols and the solid line are the same as in Figure 3.

Fig. 6. Ratio between the pressure in the hot zones, P_e(hz), and the pressure in the cold zones, P_e(cz), as a function of log(C/O) derived from RLs. The symbols and the solid line are the same as in Figure 3. The dashed line shows where C/O = 0.5, representative of the solar C/O value (Allende Prieto et al. 2002).

has a relatively low density and it is possible to increase the accuracy of the n_e(O II) determination with additional observations.

Of these four objects only one, Hu 2-1 has a high ADF of 5.05. In contrast, the other three have relatively low ADF values: 2.08 for Cn 1-5, 1.80 for M 1-61, and 1.81 for Pe 1-1. These values are smaller than the ADF average of the other sixteen objects, which amounts to 2.75, and we consider unlikely the presence of high density knots of low temperature in these three objects.

8. NGC 6153

Among our sample of 20 PNe the one with the highest ADF values is NGC 6153. This object shows $T(\text{Bac}) = 6080$ K and $T(\text{O II}) = 5780$ K, values that are very similar and considerably smaller than $T[\text{O III}] = 9120$ K, (see Tables 2 and 3). In addition, the large variations in the ratio of the 4363 to F1 [O III] line intensities as a function of velocity indicate the presence of very large temperature variations within the nebula (Barlow et al. 2006).

The densities and temperatures derived from the recombination lines of O II rule out models with densities of 2×10^6 cm^{-3}, and also models with H depleted material with temperatures of about 500 K discussed by Liu et al. (2000).

Moreover, Péquignot et al. (2002) have presented a two phase photoionization model for this object where component one, C1, has a $T_e \approx 10^3$ K and an $n_e \approx 4 \times 10^4$ cm^{-3} and component two, C2, has a $T_e \approx 6 \times 10^3$ K and an $n_e \approx 5 \times 10^3$ cm^{-3}. The gas pressures in C1 and C2 are generally found within a factor of two of each other approximately in pressure equilibrium. The O II temperatures and densities derived by us for NGC 6153 from observations, see Table 2, are in disagreement with this model and therefore rule it out.

Similarly Yuan et al. (2011) present a two phase model for NGC 6153 that approximately represents many of the observed lines. In this model the emission of the O II lines comes mostly from metal rich inclusions with $T_e = 815$ K and $n_e = 6680$ cm^{-3}. While this model does a reasonable job of reproducing most of the observed line intensities, it fails to reproduce the observed $I(4649)/I(\text{VI})$ ratio: (a) the ratio for the model presented in the paper is 0.400, the high density limit (probably the model does not include the non-LTE atomic physics required by these densities); (b) even if it were considered, the expected line intensity ratio $I(4649)/I(4638+51+61) = 1.189$ for the sum of the components of the bi-abundance model, while the observed ratios by (Liu et al. 2000) is 1.058 (Liu et al do not present errors, but by studying other faint lines with known intensity ratios, we estimate the error in this ratio to be approximately 4.5%). The electron density required to produce this line ratio, at 815 K, is $n_e = 2200^{+600}_{-400}$ cm^{-3}.

A modification to the Yuan et al. (2011) model, necessary to maintain their abundances and temperatures, is to consider metal rich inclusions 3 times less dense and 3 times more massive. This model would have the capacity to reproduce the observed O II V1 as well as the observed [O III] lines. In this model, most of the oxygen would be in the metal rich inclusions. However the observed intensity of O II $\lambda4649$ has two unfortunate consequences for this model: (a) the elec-
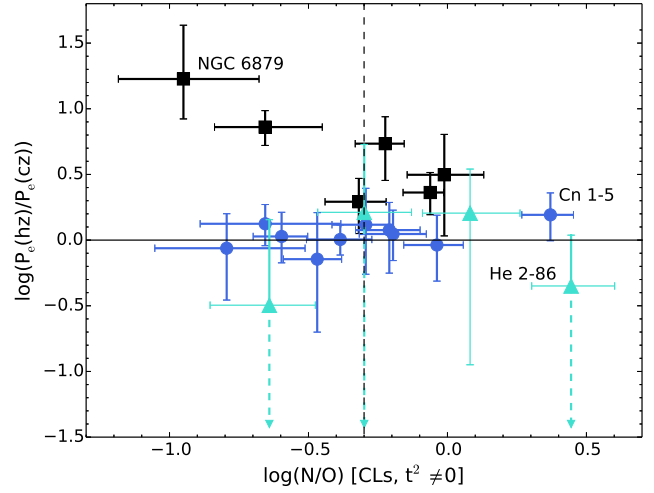

Fig. 7. Ratio between the pressure in the hot zones, $P_e(\text{hz})$, and the pressure in the cold zones, $P_e(\text{cz})$, as a function of the abundance ratios $\log(\text{N/O})$ derived from CLs for $t^2 \neq 0$. The symbols and the solid line are the same as in Figure 3. The dashed line shows where $\log(\text{N/O}) = -0.3$ which distinguishes Type I and Type II PNe according to Peimbert (1990).

tron density of the metal rich inclusions would be lower than the one from the ambient medium and (b) the pressure of the metal rich inclusions would be about a factor of 20 lower than that of the ambient medium; it is difficult to imagine a scenario that would allow such inclusions to be formed and to survive without being mixed or compressed by the ambient medium.

Overall, a bi-abundance scenario where the abundance of the cold metal rich inclusions have high density is ruled out by the observed OII V1 line ratios, and a scenario where the cold metal rich inclusions have low density has to be thought carefully before being considered.

This discussion could be extended for most objects of our sample (at least 16). Difficulties with bi-abundance models will be greater for objects where the measured $n_e(\text{O II})$ is smaller than the $n_e([\text{Cl III}])$.

9. CONCLUSIONS

We have studied a sample of 20 PNe that have been observed with high spectral resolution and high quality line intensity determinations. The main conclusions of our work follow.

(1) We have found that the determination of the $n_e(\text{O II})$ values is a very important tool to test the existence of objects with metal-rich inclusions embedded in a lower density medium.

(2) In sixteen of the objects the O II lines originate in low density regions, or, in other words they do not have high density clumps producing most of the O II line intensities.

TABLE 7

IONIC ABUNDANCES[a], ICF(N$^+$/O$^+$), AND log(N/O) VALUES FROM CLS.

Object	{N$^+$} $t^2 = 0$	{N$^+$} $t^2 \neq 0$	{O$^+$} $t^2 = 0$	{O$^+$} $t^2 \neq 0$	ICF	log(N/O) $t^2 = 0$	log(N/O) $t^2 \neq 0$
Cn 1-5	8.01±0.03	8.17±0.03	8.04±0.06	8.25±0.06	$3.31^{+0.41}_{-0.26}$	$0.50^{+0.16}_{-0.14}$	$0.44^{+0.16}_{-0.14}$
He 2-86	7.58±0.05	7.76±0.05	$7.73^{+0.11}_{0.09}$	$7.97^{+0.11}_{-0.09}$	$3.77^{+0.45}_{-0.29}$	$0.43^{+0.18}_{-0.17}$	$0.37^{+0.18}_{-0.17}$
Hu 1-1	7.53±0.03	7.68±0.03	$7.92^{+0.04}_{0.05}$	$8.13^{+0.04}_{-0.05}$	$0.95^{+0.38}_{-0.24}$	$-0.41^{+0.14}_{-0.12}$	$-0.47^{+0.14}_{-0.12}$
Hu 2-1	$7.05^{+0.05}_{-0.04}$	$7.39^{+0.05}_{-0.04}$	$7.73^{+0.21}_{-0.12}$	$8.17^{+0.21}_{-0.12}$	$1.38^{+0.33}_{-0.21}$	$-0.53^{+0.17}_{-0.22}$	$-0.64^{+0.17}_{-0.22}$
M 1-25	7.99±0.04	8.15±0.04	8.41±0.08	8.62±0.08	$1.80^{+0.31}_{-0.20}$	$-0.16^{+0.14}_{-0.12}$	$-0.22^{+0.14}_{-0.12}$
M 1-30	8.33±0.04	8.56±0.04	$8.59^{+0.09}_{-0.08}$	$8.90^{+0.09}_{-0.08}$	$1.95^{+0.23}_{-0.14}$	$0.03^{+0.11}_{-0.10}$	$-0.05^{+0.11}_{-0.10}$
M 1-61	7.23±0.04	7.38±0.04	$7.66^{+0.10}_{-0.09}$	$7.87^{+0.10}_{-0.09}$	$3.73^{+0.45}_{-0.29}$	$0.14^{+0.18}_{-0.17}$	$0.08^{+0.18}_{-0.17}$
M 3-15	6.92±0.05	7.13±0.05	$7.48^{+0.08}_{-0.09}$	$7.76^{+0.08}_{-0.09}$	$4.06^{+2.7}_{-0.12}$	$0.07^{+0.57}_{-0.09}$	$-0.02^{+0.57}_{-0.09}$
NGC 2867	6.93±0.03	7.16±0.03	7.44±0.06	7.75±0.06	$0.86^{+0.45}_{-0.29}$	$-0.58^{+0.17}_{-0.16}$	$-0.66^{+0.17}_{-0.16}$
NGC 5189	$7.85^{+0.03}_{-0.04}$	$8.01^{+0.03}_{-0.04}$	7.76±0.06	$7.98^{+0.06}_{-0.05}$	$0.86^{+0.41}_{-0.26}$	$0.03^{+0.15}_{-0.14}$	$-0.03^{+0.15}_{-0.14}$
NGC 5307	$5.98^{+0.01}_{-0.02}$	$6.14^{+0.01}_{-0.02}$	$6.73^{+0.06}_{-0.05}$	$6.96^{+0.06}_{-0.05}$	$1.06^{+2.7}_{-0.12}$	$-0.74^{+0.57}_{-0.08}$	$-0.80^{+0.57}_{-0.08}$
NGC 6153	7.19±0.03	7.61±0.03	7.41±0.05	8.01±0.05	$1.03^{+0.47}_{-0.30}$	$-0.22^{+0.17}_{-0.16}$	$-0.38^{+0.17}_{-0.16}$
NGC 6803	7.35±0.03	7.58±0.03	7.55±0.06	7.85±0.06	$1.17^{+0.47}_{-0.30}$	$-0.13^{+0.17}_{-0.16}$	$-0.21^{+0.17}_{-0.16}$
NGC 6879	5.62±0.03	5.94±0.03	$6.54^{+0.06}_{-0.05}$	$6.97^{+0.06}_{-0.05}$	$1.21^{+2.7}_{-0.12}$	$-0.84^{+0.57}_{-0.07}$	$-0.95^{+0.57}_{-0.07}$
NGC 6891	6.35±0.03	6.43±0.03	$7.14^{+0.04}_{-0.05}$	$7.25^{+0.04}_{-0.05}$	$4.16^{+2.7}_{-0.12}$	$-0.16^{+0.57}_{-0.06}$	$-0.20^{+0.57}_{-0.06}$
NGC 7009	6.54±0.02	6.85±0.02	$7.09^{+0.04}_{-0.03}$	$7.50^{+0.04}_{-0.03}$	$0.98^{+2.7}_{-0.12}$	$-0.55^{+0.57}_{-0.06}$	$-0.66^{+0.57}_{-0.06}$
NGC 7026	$7.63^{+0.04}_{-0.03}$	$7.88^{+0.04}_{-0.03}$	$7.85^{+0.14}_{-0.06}$	$8.19^{+0.14}_{-0.06}$	$0.97^{+0.43}_{-0.27}$	$-0.23^{+0.16}_{-0.19}$	$-0.32^{+0.16}_{-0.19}$
PB 8	7.16±0.03	7.39±0.03	7.92±0.07	8.23±0.07	$3.59^{+0.43}_{-0.28}$	$-0.20^{+0.16}_{-0.15}$	$-0.29^{+0.16}_{-0.15}$
PC 14	6.88±0.03	7.05±0.03	$7.49^{+0.06}_{-0.05}$	$7.72^{+0.06}_{-0.05}$	$1.18^{+0.47}_{-0.30}$	$-0.53^{+0.17}_{-0.16}$	$-0.60^{+0.17}_{-0.16}$
Pe 1-1	$7.38^{+0.09}_{-0.06}$	$7.53^{+0.09}_{-0.06}$	$7.93^{+0.22}_{-0.14}$	$8.14^{+0.22}_{-0.14}$	$1.99^{+0.40}_{-0.26}$	$-0.25^{+0.19}_{-0.21}$	$-0.31^{+0.19}_{-0.21}$

[a] {X^{+i}} = 12 + log(X^{+i}/H$^+$).

(3) For four objects of the sample, Cn 1-5, Hu 2-1, M 1-61, and Pe 1-1, the $I(4649)/I(4639+51+62)$ ratio error bars reach the high density limit and therefore, we were not able to obtain reliable values of the densities where the O II lines originate.

(4) There are two results that indicate that in the PNe of the sample H, He and O are well mixed: (a) For a subsample of 19 objects the average T_e(V1/F1) amounts to 7610 K, similar to the average T_e(Bac/Pac) which amounts to 8030 K. (b) For a subsample of 12 objects the average t^2(O^{++}) amounts to 0.045, similar to the average t^2(He$^+$/CL), which amounts to 0.042.

(5) The observed t^2(O^{++}) values, which are in the 0.024 to 0.128 range, are considerably higher than the predicted t^2(O^{++}) values by photoionization models, which are lower than 0.012. This result implies that in addition to photoionization other sources of energy are needed to explain the observed t^2(O^{++}) values. For the objects where the pressure from CLs is higher than the pressure from RLs, we suggest that shock waves could be the main cause for the high t^2(O^{++}) observed values.

(6) For many PNe of low density we find P_e(CLs)/P_e(RLs) closer to 1 than for PNe of high density; a similar result is found for H II regions. Pre-

sumably the PNe and H II regions with lower densities are older and presumably the effect of shocks becomes smaller as a function of time.

(7) For most of the PNe of our sample we find that the n_e(O II) values are similar to the n_e([Cl III]) ones. In addition we find that the volume where the bulk of the O II RLs originate is similar to the volume where the bulk of the [O III] lines originate. These two results are contrary to the models that postulate the presence of pockets of high density and low temperature embedded in a medium of lower density and higher temperature.

(8) Based on the $I(4649)/I(4639+51+61)$ ratio of multiplet V1 of O II (see Figure 3 of PP13) we find that the use of lower temperatures than the ones adopted in this paper for the O II zone implies lower n_e(O II) values than the ones presented in Table 2. This would strengthen Conclusion 7.

REFERENCES

Allende Prieto, C., Lambert, D. L., & Asplund, M. 2002, ApJ, 573, L137

Barlow, M. J., Hales, A. S., Storey, P. J., Liu, X.-W., Tsamis, Y. G., & Aderin, M. E. 2006, Planetary Nebulae in our Galaxy and Beyond (IAU Symp. 234), ed. R. H. Méndez and M. J. Barlow (Cambridge: Cambridge Univ. Press), 227

Bastin, R. J., & Storey, P. J. 2006, Planetary Nebulae in our Galaxy and Beyond (IAU Symp. 234), ed. R. H. Méndez and M. J. Barlow (Cambridge: Cambridge Univ. Press), 369

Butler, K., & Zeippen, C. J. 1989, A&A, 208, 337

Delgado-Inglada, G., Morisset, C., & Stasińska, G. 2014, MNRAS, 440, 536

Esteban, C., Peimbert, M., García-Rojas, J., et al. 2004, MNRAS, 355, 229

Fang, X., & Liu, X.-W. 2011, MNRAS, 415, 181
_____. 2013, MNRAS, 429, 2791

Ferland, G. J., Porter, R. L., van Hoof, P. A. M., et al. 2013, RevMexAA, 49, 137

García-Rojas, J., Esteban, C., Peimbert, M., et al. 2004, ApJS, 153, 501

García-Rojas, J., Esteban, C., Peimbert, A., et al. 2005, MNRAS, 362, 301

García-Rojas, J., Esteban, C., Peimbert, M., et al. 2006, MNRAS, 368, 253

García-Rojas, J., Esteban, C., Peimbert, A., et al. 2007, RevMexAA, 43, 3

García-Rojas, J., Peña, M., Morisset, C., Mesa-Delgado, A., & Ruiz, M. T. 2012, A&A, 538, A54

García-Rojas, J., Peña, M., & Peimbert, A. 2009, A&A, 496, 139

Karakas, A. I. 2010, MNRAS, 403, 1413

Kisielius, R., Storey, P. J., Ferland, G. J., & Keenan, F. P. 2009, MNRAS, 397, 903

Liu, X. 2006, Planetary Nebulae in our Galaxy and Beyond (IAU Symp. 234), ed. R. H. Méndez and M. J. Barlow (Cambridge: Cambridge Univ. Press), 219

_____. 2012, Planetary Nebulae: An Eye to the Future (IAU Symp. 283), eds. A. Manchado, L. Stanghellini, & D. Schönberner (Cambridge: Cambridge Univ. Press), 131

Liu, X.-W., Storey, P. J., Barlow, M. J., Danziger, I. J., Cohen, M., & Bryce, M. 2000, MNRAS, 312, 585.

Luridiana, V., Morisset, C., & Shaw, R. A. 2012, Planetary Nebulae: an Eye to the Future (IAU Symp. 283), 422

Mendoza, C., & Zeippen, C. J. 1982a, MNRAS, 198, 127
_____. 1982b, MNRAS, 199, 1025

Peimbert, A., & Peimbert, M. 2005, RevMexAA(SC), 23, 9

_____. 2013, ApJ, 778, 89 (PP13)

Peimbert, A., Peimbert, M., & Ruiz, M. T. 2005, ApJ, 634, 1056

Peimbert, A., Peña-Guerrero, M. A., & Peimbert, M. 2012, ApJ, 753, 39

Peimbert, M. 1967, ApJ, 150, 825

Peimbert, M. 1990, Reports on Progress in Physics, 53, 1559

Peimbert, M., & Costero, R. 1969, Bol. Obs. Tonantzintla y Tacubaya, 5, 3

Peimbert, M., & Peimbert, A. 2006, Planetary Nebulae in our Galaxy and Beyond (IAU Symp. 234), ed. R. H. Méndez, & M. J. Barlow (Cambridge: Cambridge Univ. Press), 227

Péquignot, D., Amara, M., Liu, X.-W., et al. 2002, RevMexAA(SC), 12, 142

Ramsbottom, C. A., & Bell, K. L. 1997, Atomic Data and Nuclear Data Tables, 66, 65

Ruiz, M. T., Peimbert, A., Peimbert, M., & Esteban, C. 2003, ApJ, 595, 247

Storey, P. J. 1994, A&A, 282, 999

Storey, P. J., Sochi, T., & Badnell, N. R. 2014, MNRAS, 441, 3028

Storey, P. J., & Zeippen, C. J. 2000, MNRAS, 312, 813

Tayal, S. S., & Zatsarinny, O. 2010, ApJS, 188, 32

Wesson, R., Liu, X.-W., & Barlow, M. J. 2005, MNRAS, 362, 424

Wiese, W. L., Fuhr, J. R., & Deters, T. M. 1996, JPCRD, Monograph 7, Atomic transition probabilities of carbon, nitrogen, and oxygen: a critical data compilation. (NY: AIP Press)

Yuan, H.-B., Liu, X.-W., Péquignot, D., et al. 2011, MNRAS, 411, 1035

Zeippen, C. J. 1982, MNRAS, 198, 111

Gloria Delgado-Inglada, Antonio Peimbert, Manuel Peimbert, and Miriam Peña: Instituto de Astronomía, Universidad Nacional Autónoma de México, Apdo. Postal 70-264. México, 04510 D. F., Mexico (gdelgado, antonio, peimbert, miriam@astro.unam.mx).

J. García-Rojas: Instituto de Astrofísica de Canarias (IAC), 38200, La Laguna, Tenerife, Spain; Universidad de La Laguna, Dept. Astrofísica, 38206, La Laguna, Tenerife, Spain (jogarcia@iac.es).